Astron. Astrophys. 281, 565–575 (1994)

ASTRONOMY AND ASTROPHYSICS

Mutual phenomena of the Galilean satellites: an analysis of the 1991 observations from VBO

R. Vasundhara

Indian Institute of Astrophysics Bangalore 560034 India

Received June 3, accepted August 3, 1993

Abstract. Results of analysis of seventeen mutual events, of the Galilean satellites, observed at the Vainu Bappu Observatory (VBO) during 1991 are presented. The light curves were fitted with theoretical models to derive the relative astrometric positions of the satellites. The dependence of the derived parameters on the various light scattering laws are investigated. Results of the analysis indicate that for Io fits using Minnaert's and Lommel-Seeliger's laws are comparable however the Lambert's law solution fails to give good fit at the centre and at the wings of the light curves. The mean value of the Minnaert's parameter for this satellite derived from the good quality occultation of light curves in the I band is 0.559 ± .011. Analysis of occultation light curves of 2O1 events using model with albedo variations inferred from Voyager imagery lead to best fit. An average residual of −340±10 km in the position of Io along its track relative to Europa compared to the E–3 ephemeris is noticed.

Key words: planets and satellites: individual: Galilean satellites – astrometry – eclipses – occultations

1. Introduction

Twice during its orbital period of about 11.6 yr, the equatorial plane of Jupiter sweeps across the sun and the inner solar system. For a few months around this period, the Galilean satellites frequently eclipse and occult each other. Since these satellites do not have atmospheres, observations of the mutual events provide accurate means of determining the relative astrometric positions of the satellite pairs. The first photoelectric observations of mutual phenomena were made in 1973 (Aksnes & Franklin 1976; Arlot et al. 1974). Observations of these events have gained importance thanks to campaigns and their predictions (Arlot 1978, 1984, 1990; Aksnes & Franklin 1984, 1990). The mutual phenomena of 1973, 1979, 1985, 1991 series have been observed extensively (Aksnes et al 1984; Arlot et al 1982; Arlot et al.1989a,b; Blanco 1988; Descamps & Thuillot 1992; Descamps et al. 1992; Franklin 1991 & GSO; Froeschle et al. 1988; Vasundhara 1991 - hereafter paper I; Mallama 1992).

The technique of extracting astrometric information from the light curve has also evolved over the past twenty years. Aksnes & Franklin (1976) described a detailed model to calculate the light loss during a mutual eclipse using a uniform disc model. Wasserman et al. (1976) discussed the importance of including appropriate limb darkening and albedo variations. Aksnes et al. (1986) showed that the longitude discrepancy of mutual satellite phenomena could be resolved if the separation of the light centre from the geometric centre was taken into account. In paper I, we have used the mutual eclipse data of 1985 to model the light curves using uniform disc, Lambert's law and Lommel-Seeliger's law, for the light distribution on the surface of eclipsed satellite. Analysis with limited data indicated that Lommel-Seeliger's law yielded better fit to the observations. Mallama (1992) analyzed the light curve of 1991 eclipse season using Minnaert's law and albedo variations inferred from Voyager images. Descamps & Thuillot (1992) used the mutual occultation light curves to derive Hapke's parameters in addition to obtaining the astrometric quantities. Observations of the mutual occultation of Io in the infrared region have been used to investigate the hot spots on its surface (Goguen et al.1988, Descamps et al.1992). This paper presents the observations of the mutual events during 1991 at the Vainu Bappu Observatory (VBO, 78°49′.58 E, 12°34′.58 N, 725 m) and a comparative study of results using various light scattering laws.

2. Data acquisition

The light collectors used in the present study were the 75 cm, 102 cm and 234 cm reflectors in cassegrain mode. The recording system consisted of a refrigerated EMI 9658 phototube and a locally built PC based pulse counting unit with a buffer memory of 16 K data points (Srinivasan et al. 1993). The observations commenced whenever possible, at least an hour before the event and were continued for another hour after the event.One of the chief sources of error in determining the depth of the events is the uncertainty in the estimation of the contribution of the sky

Send offprint requests to: R. Vasundhara

background in the focal plane diaphragm. Two dimensional detector arrays like the CCD receptors and video cameras allow accurate modelling of the sky background around the satellites (Colas & Laques 1990; Mallama 1992; Nakamura & Shibasaki 1990; Thuillot et al. 1990). While using a conventional photometer the best that is possible is to measure the sky by positioning the diaphragm at four locations equally spaced along east, west, north and south from the satellites. The sky background itself can be reduced due to its λ^{-1} and λ^{-4} dependence by carrying out the observations in the longer wave length bands. Therefore the present series of observations were carried out either through R or I filter of the Fernie's system along with a neutral density filter. On the 102 cm refractor 9 or 12 arcsecond diaphragms were used while on the 234 cm and 75 cm telescopes larger diaphragms of 18 and 30 arcsecond respectively were used.

During the eclipse events close to the date of opposition of Jupiter and during all the occultation events, both the satellites due to their proximity in the sky plane will have to be accommodated in the same focal plane diaphragm. In order to remove the contribution of the occulting or the eclipsing satellite, the relative contribution of the two satellites to the total light should be carefully estimated. The magnitude of the satellites depend on their orbital longitude and the wavelength of observations (Morrison et al. 1974). The two satellites were therefore observed individually when they were separate, just before and/or after the event. The main occultation or eclipse events were monitored continuously. The integration time was selected such that the entire event and the four sets of sky measurements before and after the events were captured in the buffer of 16 K data points. The integration times therefore, ranged between 0.15 seconds to 0.3 seconds. The integration times for the longer events were set between 0.8 – 1.0 sec. While monitoring events longer than one hour, another satellite, mostly Callisto was observed several times to check the sky transparency variations.

The light curves will appear in the Catalogue of the observations of mutual phenomena made in 1991 during the PHEMU91 campaign (Arlot et al. 1993)

3. Determination of time of light minimum

The time of light minimum T_l was determined by folding as discussed in paper I or by fitting a third degree polynomial to the deep part of the light curve. The method of folding was used for continuous light curves. Light curves with breaks either due to clouds or while centering the object were analyzed by polynomial fit. The time of light minimum were also estimated from the theoretical light curve that best fitted the observations, this being the only method by which T_l of the two overlapping 2O1 and 2E1 events on 91/01/29 could be estimated. The complex geometry during the 2O3 event on 91/01/23 resulted in a broad light curve the minimum of which could not be determined due to interruptions by clouds. Table 1 gives the journal of observations; column (2) gives the time of light minimum as determined by folding or polynomial fit. Column (3) gives the fitted time of light minimum. The maximum light loss estimated by fitting a third degree polynomial to the deep part of the light curve are given in column (4). The telescope aperture, filter used, and the air mass at T_l are given in columns (5) – (7) respectively. The sky conditions at the time of observations are indicated in column (8); an entry of 1 indicates good sky condition and 3 as variable transparency. The uncertainty in the light loss was determined from the uncertainty in determination of sky counts, uncertainty in determining the raw counts outside and during the event, uncertainty in estimating the extinction coefficient and the uncertainty in estimating the relative contribution of the occulting/eclipsing satellite to total light, using the standard method (Bevington 1969).

4. Comparison of observations with theory

4.1. Calculation of the event geometry

The theoretical light curves were constructed by computing the light loss at each instant corresponding to the instantaneous separation between the centres of the occulted (S2) and occulting (S1) satellites for occultations and the distance of eclipsed satellite (S2) from the shadow axis for eclipses. The joviocentric positions and velocities of the satellites were computed using E-3 ephemeris (Lieske 1977, 1987). The radii of Io, Europa, Ganymede and Callisto were taken to be 1815, 1569, 2631 and 2400 km respectively (Morrison 1982). Detailed geometry for computing light loss under the umbra and penumbra has been described in paper I. The occultation geometry was computed in a similar manner taking topocentric aspect. For eclipses the correction for light travel time between the two satellites and the observer were taken into account by combining the position of observer at the time of observation (T_{obs}) with that of the position of the eclipsed satellite at time (T_{s2}) and the position of the eclipsing satellite at time (T_{s1}), where

$$T_{s2} = T_{obs} - R_{o2}/c$$

$$T_{s1} = T_{s2} - (R_{s2} - R_{s1})/c, \quad (1)$$

where c is the velocity of light, R_{o2} is the ' observer – S2 ' distance, R_{s2} and R_{s1} are the ' Sun – S2 ' and ' Sun – S1 ' distances respectively . For occultation events the light time correction was taken into account by taking the position of S2 at time T_{s2} when the beam of light which reflected out from its surface at this instant reached the observer at time T_{obs}, and the position of S1 at time T_{s1} when it intercepted this beam. The observer's position was taken at time T_{obs}, hence

$$\begin{aligned} T_{s2} &= T_{obs} - R_{o2}/c \\ T_{s1} &= T_{s2} + (R_{o2} - R_{o1})/c \\ &= T_{obs} - R_{o1}/c, \end{aligned} \quad (2)$$

where R_{o1} is the ' observer – S1 ' distance.

Table 1. Observed times of light minimum, light loss[a] and journal of observations

UTC Date Event	T_l Observed	T_l Fitted	Light loss	Telescope Aperture (cm)	Filter	Airmass	Observing condition
(1)	(2)	(3)	(4)	(5)	(6)	(7)	(8)
91/01/22	18:23:12.7	18:23:13.0	0.721	102	R	1.04	1
2E1	+0.5s		±.01				
91/01/22	18:43:52.5	18:43:51.1	0.411	102	R	1.02	1
2O1	±0.5s	-	±.01				
91/01/23[b]	-	-	0.358	102	R	1.29	2
2O3			±.015				
91/01/29	–	21:00:27.0	0.651	234	R	1.18	1
2O1			±.02				
91/01/29	–	21:03:23.9	0.572	234	R	1.18	1
2E1			±.02				
91/02/05	23:13:27.0	23:13:22.4	0.721	102	I	2.86	3
2O1	±10.0s		±.04				
91/02/16	14:29:41.9	14:29:50.1	0.685	102	I	1.41	1
2O1	±0.5s		±.003				
91/02/16	15:18:31.7	15:18:31.9	0.726	102	I	1.18	1
2E1	±0.5s		±.01				
91/02/23	16:39:16.1	16:39:15.0	0.685	102	I	1.01	1
2O1	±0.5s		±.01				
91/02/23	17:42:58.5	17:42:58.5	0.739	102	I	1.02	1
2E1	±0.5s		±.01				
91/03/09	20:58:40.5	20:58:41.7	0.386	102	I	2.81	2
2O1	±1.5s		±.03				
91/03/18	19:43:25.1	19:43:21.8	0.243	75	I	2.11	2
4E2	±3s		±.01				
91/03/20	13:55:45.3	13:55:45.4	0.635	102	I	1.46	2
2E1	±1.0s		±.01				
91/03/27	14:26:37.3	14:26:40.2	0.106	102	I	1.01	1
2O1	±0.5s		±.01				
91/03/27	16:14:11.7	16:14:12.0	0.546	102	I	1.07	1
2E1	±0.5s		±.003				
91/04/03	18:31:49.0	18:31:49.5	0.405	75	I	2.05	3
2E1	±2.0s		±.011				
91/05/17	14:49:41.7	14:49:42.5	0.772	102	I	1.42	2
1E2	±1.5s		±.006				

a. After removing the contribution from the occulting/eclipsing satellite.
b. T_l not derived due to complexity of the light curve and presence of clouds.

4.2. Estimation of theoretical light loss

4.2.1. Model using uniform albedo distribution

The light loss during an occultation is equal to that reflected from the regions on $S2$ blocked by $S1$ and is given by,

$$L_o = \int\int wi.I(\mu_0, \mu, \alpha).da_e, \quad (3)$$

where da_e is an elementary area on the disc of the satellite as viewed from the earth. The weight factor wi is 1 for illuminated regions and 0 for regions beyond the terminator. The integration was carried out over the occulted regions on the satellite. For an eclipse the loss in light in the penumbra and umbra are given by,

$$L_e = \int\int l_p.wi.I(\mu_0, \mu, \alpha).da_e + \int\int wi.I(\mu_0, \mu, \alpha).da_e, \quad (4)$$

where $(1 - l_p)$ is the intensity of light in the penumbra at the location of the elementary area da_e which was estimated by computing the fractional area of the unocculted portion on the apparent limbdarkened disc of the Sun at the distance of the eclipsing satellite. The integrations were carried out using 12 step Gaussian quadrature. The loss in light was then scaled in the range 0−1 by normalizing with respect to the light from the uneclipsed or unocculted satellite .

The photometric function $I(\mu_0, \mu, \alpha)$ in Eqs. (3) and (4) is the flux from a point on the surface of the satellite which

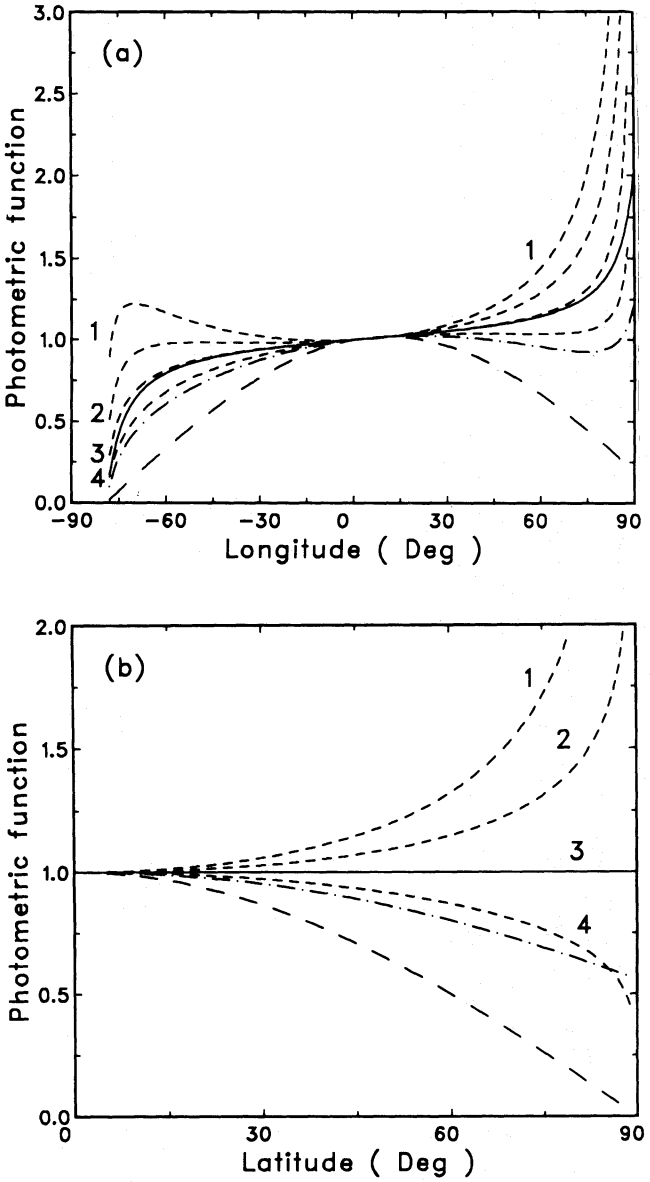

Fig. 1. a and b. Variation of the photometric function along the equator **a** and along the central meridian **b** for a solar phase angle of 11°. The continuous line is for Lommel-Seeliger's law; the long dashed line for Lambert's law; the dotted dashed line for Hapke's law for parameters for Io from Descamps & Thuillot (1992); and the short dashed lines-Minnaert's law. For Minnaert's curves the labels 1–4 refer to values of $k(\alpha)$ from 0.3–0.6

is illuminated at an angle $\cos^{-1}(\mu_0)$ and viewed at an angle $\cos^{-1}(\mu)$ to the surface normal. Alpha is the solar phase angle . It is assumed that the entire surface of the satellite has the same average albedo. Expressions have been worked out by various authors to explain the observed reflectance of solar system objects without atmosphere. Some of these are empirical relations (Hapke 1963; Irvine 1966; Minnaert 1941). Scattering laws for particulate surfaces of arbitrary albedo have been derived from radiative transfer by Lumme & Bowel (1981), Goguen (1981),

Table 2. Brightness ratios and boundaries used in the model for Io

Region	Latitude (b) on Io (deg)	Relative brightness in R and I bands
Equatorial	$0 < \|b\| < 50$	0.85 (sub-Jupiter face) 0.90 (anti-Jupiter face)
Polar	$60 < \|b\|$	0.49
Overlapping	$50 < \|b\| < 60$	0.5 Equatorial + 0.5 polar

Scattering law : Minnaert's law

Table 3. Features modelled on Ganymede

Feature	Relative[a] brightness
Perrine	0.765
Nicholson east and west	0.765
Bright ray Crater *Tros*	1.28
Bright Polar Caps	1.16

Scattering law : Lunar like (Lommel-Seeliger's law)
Relative brightness of deafault regions = 0.86

a. Adapted from Squyres and Veverka (1981)

and Hapke (1981). The scattering laws used in the present study are given below:

1) Photometric function for lunar like surfaces developed by Hapke (1963) and Irvine (1966) which correctly describe the scattering from a dark porous surface like that of the moon is given by

$$I(\mu_0, \mu, \alpha) = F\left(\frac{\mu_0}{\mu_0 + \mu}\right).f(\alpha), \quad (5)$$

where

F = incident solar flux

$f(\alpha)$ = phase function of the surface.

The expression in Eq.(5) closely approximates the scattering by many low albedo particulate materials. The angular characteristics of this function is the well known Lommel-Seeliger's law.

2) For very bright surfaces one can use Lambert's law given by

$$I(\mu_0, \mu, \alpha) = Fr_n\mu_0 \quad (6)$$

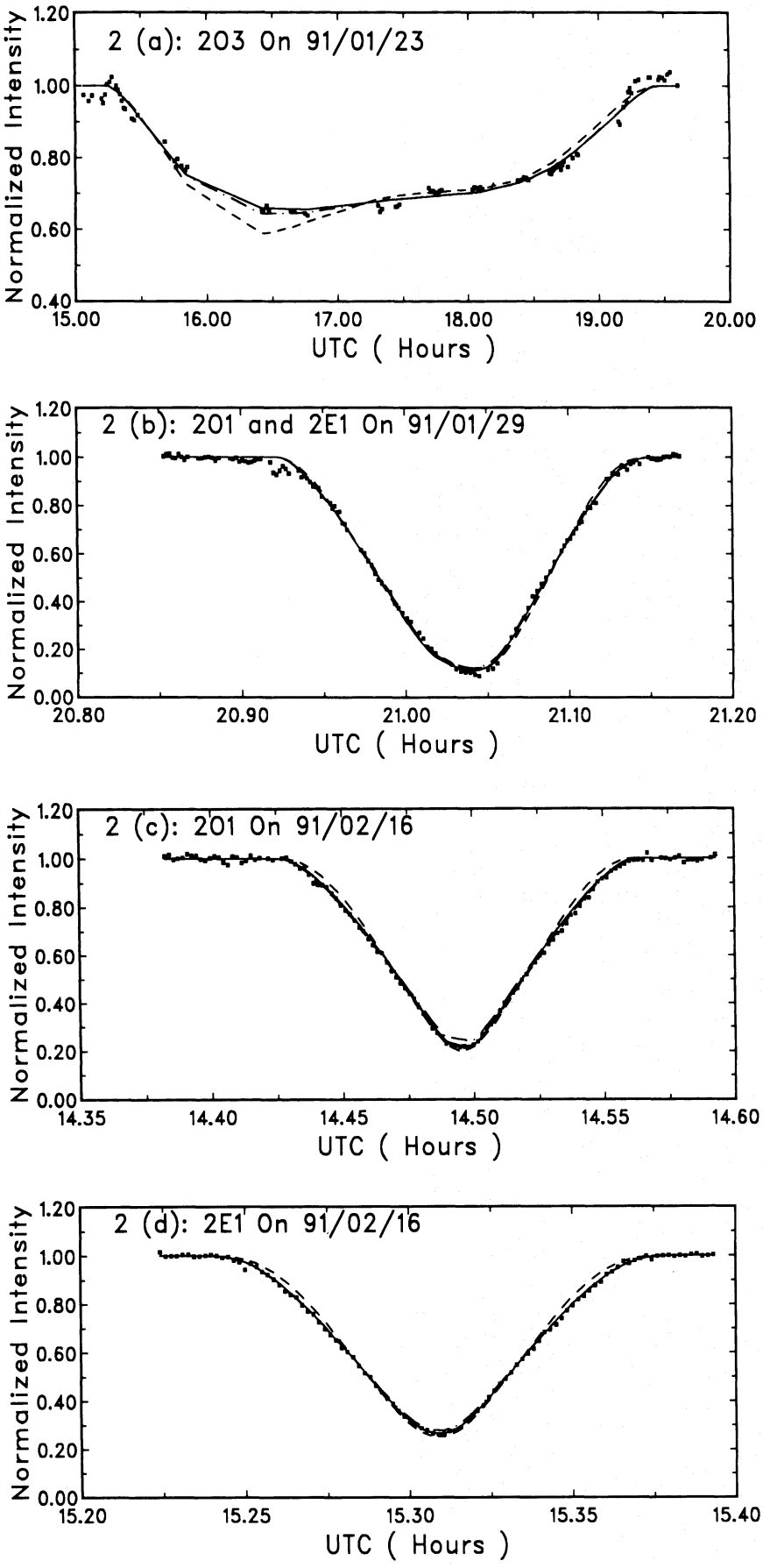

Fig. 2. a–d. Observed and fitted light curves. **a** The dot dashed line, short dashed line, and continuous line correspond to models using Lommel Seeliger's law, Lambert's law, and model (AV) in Table 3. **b,c,d** The dot dashed line, short dashed line, continuous line and long dashed line (for **b,c**) correspond to models using Lommel Seeliger's law, Lambert's law, Minnaert's law and model AV in Table 2

where r_n is the normal albedo. By definition, a Lambert surface appears equally bright when viewed from any angle and reflects all the light incident on it.

3) A widely used empirical photometric function is the Minnaert's function (Minnaert 1941) given by

$$I(\mu_0, \mu, \alpha) = FB_0(\alpha).\mu_0^{k(\alpha)}.\mu^{k(\alpha)-1} \quad (7)$$

where $B_0(\alpha)$ and $k(\alpha)$ are the two Minnaert's parameters which are functions of α and the wavelength. Goguen (1981) has shown that Eq.(7) is only a crude approximation to the scattering properties of real surfaces; however it has been found to be valid for near zero solar phase angles. Therefore Minnaert's law can be used as a convenient approximation (except very close to the limb) to study small phase angle data. Since the maximum solar phase angle at the distance of Jupiter is less than 12°, this law has been used in the present study. It has been successfully used by Simonelli & Veverka (1986a) to analyze Voyager observations of Io. In the extreme case when $k(\alpha)$ is equal to unity this represents Lambert's Law. Variation of the photometric functions along the photometric equator and meridian at a solar phase angle of 11° are shown in Figs. 1a and b respectively. The continuous line corresponds to Lommel-Seeliger's law; the long dashed line for Lambert's law; the dotted dashed line for Hapke's law (Hapke 1981) for a smooth surface using parameters for Io in the V band from Descamps & Thuillot (1992); and the short dashed lines-Minnaert's law. For Minnaert's curves the labels 1-4 refer to values of $k(\alpha)$ from 0.3-0.6.

4.2.2. Non uniform Albedo distribution

In the post Voyager era, the full potential of mutual event data can be exploited by taking into account the differences in albedo over different terrains on the surface of the satellites. Most of the events observed from VBO during the 1991 season involved occultations or eclipses of Io by Europa. Io has a broad equatorial band, with brighter white markings and brown polar regions (Simonelli & Veverka 1986a). Since the mutual event observations in the present study were through R and I filters and the Voyager imagery was carried out in the wavelength region 3500Å to 5900Å, we used the published values of the equator to pole albedo ratios derived by Simonelli & Veverka (1986a) for the orange filter observations as the starting values. Better fits were obtained for the relative brightness values given in Table 2, although no attempt was made to determine the albedo ratio between equator to pole as the free parameter. Simonelli & Veverka (1986b) have shown that the Hapke's parameters (Hapke 1984) that best fitted the observed limb darkenings on the Voyager images were different for the equatorial and polar regions. Lack of published data on these parameters in the R and I band demanded their determination as additional free parameters during the fit using a large number of occultation light curves. Paucity of available data precluded such an attempt of using Hapke's law in the present study.

For the single observation of occultation of Ganymede by Europa on 91/01/23, in addition to Lommel-Seeliger's law and Lambert's law the light curve was also fitted by modelling the

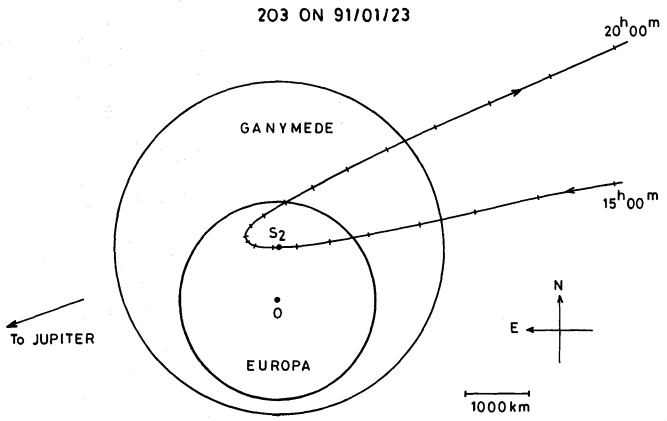

Fig. 3. Geometry during the occultation of Ganymede centered at S_2 at the instant of close approach on 91/01/23. The path of Ganymede between 15^h00^m UTC and 20^h00^m UTC is along the curved track. The tick marks indicate position of Ganymede at intervals of 15^m

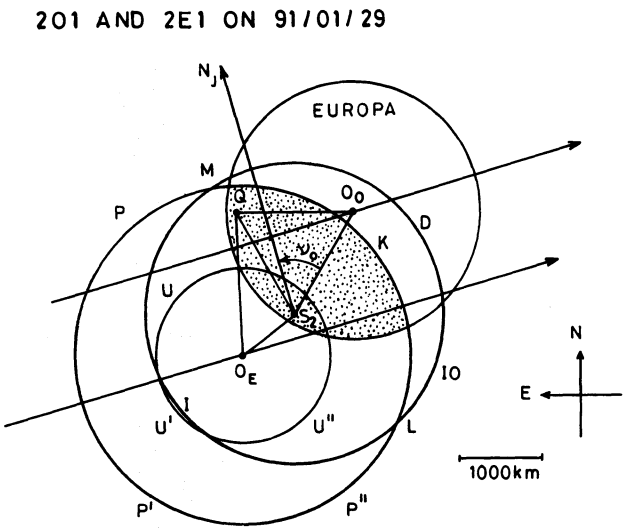

Fig. 4. Geometry during the composite occultation and eclipse events of Io by Europa on 91/01/29. The dotted area on Io (centered at S_2) is occulted by Europa (Centered at O_O) and at the same time eclipsed by the umbra $U''U'UU''$ and the penumbra $P''P'PP''$ centered at O_E. The arrows indicate direction of motion of Europa and the shadow center relative to Io

polar caps, the *regiones Nicholson west* and *east* and the bright ray crater *Tros*. The albedo ratios and boundaries were adapted from Squyres and Veverka (1981) and Mallama (1991) for the phase angle of $-1°.1$ at the time of this event. The relative values of $f(\alpha)$ on the different terrains on Ganymede used in the present study are given in Table 3.

4.3. Extraction of Astrometric parameters

The light curves were recorded with time resolutions ranging between 0.15s to 0.3s for fast events and between 0.8 to 1.0s for slow events (Sect. 2). To improve the signal to noise ratio the normalized intensity values at these time resolutions were

Table 4. Fitted parameters (eclipses)

Date	Scattering law	Event	Phase α (deg)	Impact parameter (km)	$k(\alpha)$	$\chi^2 \times 10^4$
(1)	(2)	(3)	(4)	(5)	(6)	(7)
91/01/22	L-S		−1.3	178 ± 90		0.651
	L			560 ± 40		5.466
	M			−6 ± 250	0.461	0.595
	P	2E1	Annular	220		
91/01/29	L-S		+0.2	130 ± 70		3.133
	L			511 ± 420		4.615
	M			193 ±80	0.561	3.064
	AV			283 ±50	0.543	2.876
	P	2E1	Annular	290		
91/02/16	L-S		+3.9	≃ 0.0 ±990		0.796
	L			488 ±40		3.934
	M			≃ 0.0 ±950	0.554	0.482
	P	2E1	Annular	209		
91/02/23	L-S		+5.2	≃0 ±960		1.839
	L			434 ± 40		3.698
	M			≃0 ±940	0.589	0.742
	P	2E1	Annular	86		
91/03/18	L-S		+8.7	3027 ± 40		1.116
	L			3006 ± 40		1.003
	M			3003 ± 40	1.105	1.010
	P	4E2	Penumbral	3094		
91/03/20	L-S		+8.9	−544 ± 20		1.113
	L			−766 ± 20		3.778
	M			−331 ± 30	0.310	0.627
	P	2E1	Annular	−681		
91/03/27	L-S		+9.6	−924 ± 10		0.571
	L			−1027± 10		2.192
	M			−934 ± 10	0.544	0.564
	P	2E1	Annular	−986		
91/04/03	L-S		+10.2	−1428 ± 40		6.750
	L			−1440 ± 40		9.304
	M			−1425 ± 40	0.325	6.488
	P	2E1	Partial	−1324		
91/05/17	L-S		+10.3	−795 ± 20		0.557
	L			−905 ± 20		1.675
	M			−826 ± 20	0.620	0.463
	P	1E2	Partial	−811		

binned such that the total light curve had approximately 100 data points. The observed and theoretical light curves were fitted using Marquardt's technique (Bevington 1969). The free parameters in the fit were the impact parameter y and a shift δx along the track of S2 with respect to S1 for occultations and the shadow centre for eclipses. This shift along the track is required to shift the theoretical geometric centre to the observed position of geometric centre hence

$$\delta x = (T_g - T_p)V, \tag{8}$$

is the (O–C) in relative distance between the satellites along their track, where T_p is the predicted time of close approach and V is the relative sky plane velocity. When Minnaert's law was used in the model, the Minnaert's parameter $k(\alpha)$ was also derived during the fit. For the good quality light curves the solutions converged within 3−4 iterations. The final solutions were found to be independent of the starting values. The fitted value T_l given in Table 1 was derived from the time of minimum of the fitted light curve. The fitted impact parameters for the eclipse and occcultation events are given in Tables 4 & 5 respectively. For each eclipse event there are three entries, these correspond to Lommel-Seeliger's law (L–S), Lambert's law (L) and Minnaert's law (M) respectively. For occultations the fourth entry if present corresponds to that derived from the model using

Table 5. Fitted parameters (occultations)

Date	Scattering law	Event	Phase α (deg)	Impact parameter (km)	$k(\alpha)$	$\chi^2 \times 10^4$
(1)	(2)	(3)	(4)	(5)	(6)	(7)
91/01/22	L-S		−1.3	−1411 ± 40		1.491
	L			−1430 ± 27		5.955
	M			−1405 ± 40	0.399	1.313
	AV			−1400 ± 40	0.443	1.331
	P	2O1	Partial	−1349		
91/01/23	L-S		−1.1	1021 ± 860		4.344
	L			1130 ± 90		8.659
	AV			957 ± 920		4.278
	P	2O3	Annular	836		
91/01/29	L-S		+0.2	−635 ± 70		3.133
	L			−983 ± 60		4.615
	M			−685 ± 70	0.561	3.064
	AV			−818 ± 60	0.543	2.876
	P	2O1	Partial	−974		
91/02/05	L-S		+1.7	−262 ± 240		74.1
	L			−567 ± 140		83.1
	M			68 ± 1520	0.357	72.7
	P	2O1	Partial	−558		
91/02/16	L-S		+3.9	−4 ± 205		2.381
	L			433 ± 20		5.201
	M			−13± 166	0.5821	1.454
	AV			105 ± 30	0.5064	0.853
	P	2O1	Annular	118		
91/02/23	L-S		+5.2	505 ± 40		0.586
	L			722 ± 30		3.632
	M			515 ± 40	0.516	0.584
	AV			587 ± 40	0.564	0.700
	P	2O1	Partial	590		
91/03/09	L-S		+7.5	1542 ± 110		3.583
	L			1533 ± 80		4.929
	M			1540 ± 100	0.565	3.546
	AV			1525 ± 100	0.617	3.547
	P	2O1	Partial	1525		
91/03/27	L-S		+9.6	2609 ± 50		0.961
	L			2476 ± 40		1.053
	M			2670 ± 50	0.327	0.963
	P	2O1	Partial	2523		

albedo variations (AV). The impact parameter predicted using E–3 ephemeris (P) is given for all the events.

Four of the fitted light curves are plotted in Figs. 2a–d. The goodness of fit can be assessed from the value of χ^2. The unusual shape of the light curve of the 2O3 event in Fig. 2a is due to the complex geometry shown in Fig. 3. The positions of Ganymede and Europa are shown at the instant of close approach. The relative path of Ganymede between 15^h00^m to 20^h00^m is shown along the curved track. The occultation and eclipse events on 91/01/29 which occurred close to the date of opposition (α = 0°.2) followed in quick succession. Figure 4 shows the geometry of this event. Figure 2b shows the composite light curve. The blended light curve was fitted with theoretical composite light curves which were obtained by summing the light loss on Io, in the shadow (eclipse) and behind Europa (occultation). Dotted regions which were both occulted and eclipsed were considered to be only occulted.

Table 6 gives the final results; the fitted time T_g of close approach of the geometric centre of the occulted (eclipsed) satellite to the geometric centre of the occulting satellite (shadow centre) is given in column (2) and the relative sky plane coordinates $\Delta\alpha$ cosδ and $\Delta\delta$ as seen by a terrestrial (heliocentric) observer at this instant are given in columns (7) & (8) respectively. Columns (3 & 4) give the (O–C) in time and distance compared to the E-3

Table 6. (O−C) along the track and relative astrometric positions

Date Event	T_g (UTC)	(O-C)E-3 Time (sec)	Distance (km)	Fitted T_g–T_l (sec)	Pred. ΔT_α (sec)	$\Delta\alpha cos\delta$ S2-S1 (arcsec)	$\Delta\delta$ (arcsec)	Orbital longitudes θ_1 (deg)	θ_2 (deg)
(1)	(2)	(3)	(4)	(5)	(6)	(7)	(8)	(9)	(10)
91/01/22 2E1	18:23:11.9	36.1	−323	−1.1	−1.5 −1.8	0.0163	0.0569	218	265
91/01/22 2O1	18:43:53.7	37.5	−353	2.6	1.3 1.6	-0.1326	−0.4277	219	266
91/01/23[a] 2O3	16:30:16.3	170.5	+335	–	12.8 15.3	0.0913	0.2917	312	332
91/01/29 2O1	21:00:27.0	31.5	−300	≃0	≃0.0 ≃ 0.0	−0.0619	−0.2041	219	271
91/01/29 2E1	21:03:23.9	31.7	−383	≃0	≃0.0 ≃ 0.0	0.0261	0.0870	219	271
91/02/05[b] 2O1	23:13:20.6	24.1	−230	− 1.8	−1.5 − 1.7	–	–	219	275
91/02/16 2O1	14:29:39.6	24.6	−344	−10.5	−3.0 −3.5	0.0092	0.0319	218	281
91/02/16 2E1	15:18:37.0	24.7	−366	5.1	2.9 3.3	≃ 0	≃0	218	284
91/02/23 2O1	16:39:11.0	26.9	−329	−4.0	−3.8 −4.2	0.0501	0.01764	217	284
91/02/23 2E1	17:43:02.4	20.9	−338	4.0	3.6 4.0	≃ 0.0	≃ 0.0	217	288
91/03/09 2O1	20:58:35.6	21.8	−371	−6.1	−4.6 −5.2	0.1228	0.4452	216	290
91/03/18 4E2	19:43:27.4	13.3	−255	5.6	- 4.6[c]	0.2481	0.7457	168	37
91/03/20 2E1	13:55:51.0	15.8	−319	5.6	5.1 5.4	−0.0444	−0.1341	213	300
91/03/27 2O1	14:26:34.8	18.0	−350	−5.4	−3.1 −4.3	0.1972	0.7260	214	298
91/03/27 2E1	16:14:17.8	15.0	−317	5.8	5.1 5.6	−0.0762	−0.2274	212	304
91/04/03 2E1	18:31:55.8	10.4	−231	6.3	4.8 5.3	−0.1189	−0.3509	210	307
91/05/17 1E2	14:49:46.2	−6.9	+169	3.7	4.1 4.5	−0.0700	−0.1934	225	335

a.T_l uncertain due to broad light curve
b. Astrometric positions and timings unreliable due to noisy data.
c.Penumbral event, used approximate expression (Aksnes et al.1986)

ephemeris (Lieske,1987). The observed phase correction given by $(T_g - T_l)$ is reported in column (5), where T_l is the time of light minimum of the best fitting theoretical light curve. The predicted phase corrections ΔT_α (Aksnes *et al.* 1986) are given in column (6). The first row corresponds to Lommel-Seeliger's law and the second row to Lambert's law. The orbital longitudes at mid event are given in columns (9 & 10)

5. Results and discussions

A comparison of the χ^2 values in Tables(4 & 5) indicates that fits using Minnaert's law and Lommel-Seeliger's law are comparable, however Lambert's law solution fails to give a good fit. As shown in Figs. 2c–d the large χ^2 in case of the Lambert's law solution (short dashed line) is mainly due to poor fit at the centre and at the wings. The fits using Minnaert's law (solid line) and Lommel-Seeliger's law (dot dashed line) are equally good. The long dashed lines in Figs. 2b–c correspond to the model including the albedo variations given in Table 2. This curve is not clearly discernible from the solid curve of Minnaert's law solution. The mean value of the Minnaert's parameter derived from the good quality light curves in the I band is 0.559 $\pm$ .011. Due to limited data its dependence on phase could not be evaluated. Except for the annular events, the fitted impact parameters using Lommel- Seeliger's law agree closely to those using Minnaert's law. It is to be expected because the derived value of $k(\alpha)$ is close to 0.5 (Figs. 1a,b). Therefore scattering on the surface of Io appears to be lunar like. An average residual of -340 ± 10 km in the position of Io along its track relative to Europa compared to the E–3 ephemeris is noticed. Similar trend has been reported by Mallama (1992). However as the orbital longitudes at mid event slowly drift through the mutual event season, a detailed analysis of the (O–C) in longitude as carried out by Aksnes & Franklin (1976) and (Arlot (1982) would be appropriate. The difference in the predicted phase corrections using Lommel-Seeliger and Lambert laws are less than the observational uncertainty in the determination of T_l. The fitted phase correction is found to be on most cases larger than the predicted value. A possible reason could be that the expression for the phase correction was derived by Aksnes et al. (1986) in an elegant manner for correcting T_l which was conventionally determined by the method of folding the entire light curve. Whereas the fitted phase correction corresponds to the difference in close approach times of the geometric and light centres to the target. This discrepancy is found to be pronounced for the annular events. Analysis of occultation light curves of 2O1 events on 91/01/22, 91/01/29, 91/02/16, 91/02/23 and 91/03/09 using model with albedo variations (AV) appear to yield impact parameters closer to the predicted ones within the observational uncertainty implying that the relative latitudes predicted by theory (E-3 by Lieske) is already accurate and further corrections can only be effected with realistic albedo maps. The full potential of mutual event data can therefore be harnessed by using the two dimensional arrays to improve the accuracy of measurement of light loss and using a realistic model to generate the theoretical light curves. Such a model would be preferable to the uniform albedo model for analysing especially the annular events.

Acknowledgements. I am grateful to Prof.J.C.Bhattacharyya for several useful discussions and encouragement through-out the work. I am deeply indebted to Prof.J.Lieske for providing the computer codes to calculate the joviocentric positions and velocities of the satellites along with the E-3 ephemeris. I thank Mr.N.Dinakaran for observing on the 75 cm telescope at VBO.

References

Aksnes,K., Franklin,F. 1976, AJ 81, 464
Aksnes,K., Franklin,F. 1984, Icarus 60, 180
Aksnes,K., Franklin,F. 1990, Icarus 84, 54
Aksnes,K., Franklin,F., Millis,R., et al. 1984, AJ 89, 280
Aksnes,K., Franklin,F., Magnusson,P. 1986, AJ 92, 1436
Arlot,J.E., Camichel,H., Link,F. 1974, A&A 35, 115
Arlot,J.E. 1978, A&AS 34, 195
Arlot, J.E. 1982, Ph.D. Thesis, Université Paris
Arlot,J.E., Bernard,A., Bouchet,P., Daguillon,D. Dourneau,G. 1982, A&A 111, 151
Arlot,J.E. 1984, A&A 138, 113
Arlot,J.E., Thuillot,W., D'Ambrosio,V. 1989a, A&A 213, 479
Arlot,J.E., Bouchet,P., Gouiffes,Ch., Schmeider,F.X., Thuillot,W. 1989b, AJ 98, 1890
Arlot,J.E. 1990, A&A 237, 259
Arlot,J.E., Barroso,Jr,J., Jablonsky,F.J., Quast,G.R., Thuillot,W. 1990, A&AS 82, 513
Arlot,J.E., Thuillot,W., Barroso,Jr,J., et al. 1992, A&AS 92, 151
Arlot,J.E. 1993, Private communication
Bevington,P.R., 1969. Data Reduction and Error Analysis for the physical sciences. McGraw-Hill, New York.
Blanco,C. 1988, A&A 205, 297
Colas,F. Laques,P. 1990, Proc., PHEMU91 workshop,Teramo (Eds. J.E.Arlot and R.Burchi), 29
Descamps,P., Arlot, J.-E., Thuillot, W.,et al. 1992, Icarus 100, 235
Descamps,P., Thuillot, W. 1992, *preprint*, Bureau des Longitudes, Paris, France
Franklin,F., GSO, 1991, AJ 102, 806
Froeschle,M., Helmer,G., Meyer,C. 1988, A&A 189, 277
Goguen, J.D.1981 Ph.D. Thesis, Cornell University, Ithaca, NY
Goguen, J.D., Sinton, W.M., Matson, et al. 1988, Icarus 76, 465
Hapke,B. 1963, J. Geophys. Res. 68, 4571
Hapke,B. 1966, AJ 71, 333
Hapke, B. 1984, Icarus 59, 41
Hapke, B. 1981, J. Geophys. Res. 86, 3039
Irvine,W. 1966, J. Geophys. Res. 71, 2931
Lieske, J.H. 1977, A&A 56, 333
Lieske,J. 1987, Private communication of E-3 ephemeris
Lumme,K. Bowel,E. 1981, AJ 86, 1694
Mallama,A. 1991, Icarus 92, 324
Mallama,A. 1992, Icarus 95, 309
Morrison,D. 1982,in *Satellites of Jupiter*, Ed. D.Morrison, University of Arizona press, 3.
Morrison,D., Morrison N.D., Lazarewicz,R. 1974, Icarus 23, 399
Minnaert,M. 1941, AJ 93, 403
Nakamura, T., Shibasaki, H. 1990, in Proc., PHEMU91 workshop, Teramo, Eds. J.E.Arlot & R.Burchi, 41

Simonelli,D.P., & Veverka,J. 1986a, Icarus 66, 403
Simonelli,D.P., & Veverka,J. 1986b, Icarus 68, 503
Squyres,S.W., & Veverka,J. 1981, Icarus 46, 137
Srinivasan, R., Nagaraja Naidu, B., Vasundhara, R. 1993, Indian Journal of Pure and Appl. Phys.31, 36
Thuillot, W., Arlot, J.-E., Vu, D.T. 1990, Proc., PHEMU91 workshop, Teramo, Eds. J.E.Arlot and R.Burchi, 33
Vasundhara, R. 1991, J. Astrophys. Astr.12, 69
Wasserman, L.H., Elliot, J.L., Veverka, J., 1976, Icarus 27, 91

This article was processed by the author using Springer-Verlag LaTeX A&A style file version 3.